Energy dependence of hadron spectra and yields in p+p and ^{7}Be+^{9}Be collisions from the NA61/SHINE experiment at the CERN SPS

D.T. Larsen for the NA61/SHINE Collaboration
Uniwersytet Jagielloński, Łojasiewicza 11, 30-348 Kraków, Poland
E-mail: dlarsen@cern.ch

Abstract. The NA61/SHINE programme on strong interactions covers the study of the onset of deconfinement and aims to discover the critical point of strongly interacting matter by performing an energy and system-size scan over the full CERN SPS momentum range. So far the scans of p+p, ^{7}Be+^{9}Be, as well as Ar+Sc have been completed. Results from p+p and Be+Be collisions are now emerging, in particular the energy dependence of hadron spectra and yields. Status and preliminary results from this effort will be presented.

1. Introduction

NA61/SHINE [1] is a fixed target experiment at the CERN SPS. Tracking is provided by five time projection chambers. Additionally, particle identification is aided by time-of-flight detectors. A modular calorimeter is used to determine the collision centrality for nucleus-nucleus collisions. Both primary and secondary beams are available to the experiment, allowing data taking with projectile sizes ranging from proton to lead, as well as with pions and kaons. Besides studying strong interactions, the experiment also performs precise hadron production reference measurements for neutrino (Fermilab and T2K) and cosmic-ray (KASCADE and Pierre Auger Observatory) physics.

2. Analysis of identified hadron spectra

More than 90% of primary negative particles produced in inelastic interactions at SPS energies are π^-. Thus, the π^- spectra may be obtained by subtracting the small non-pion contribution from the overall spectra for negatively charged hadrons. This non-pion contribution is taken from the EPOS model [2]. Since particle identification is not required, a very large phase-space acceptance is obtained. In addition to the h^- method [3], dE/dx and time-of-flight may be used for proper identification. The dE/dx method is based on the particle energy loss in the TPC gas, while the particle mass can be identified using the time-of-flight information. The acceptances for these methods are shown in Figure 1 for p+p interactions at 158 GeV/c. The results are corrected for detector inefficiencies, feed-down from weak decays and secondary interactions, contribution from non-target interactions, as well as trigger and event selection biases.

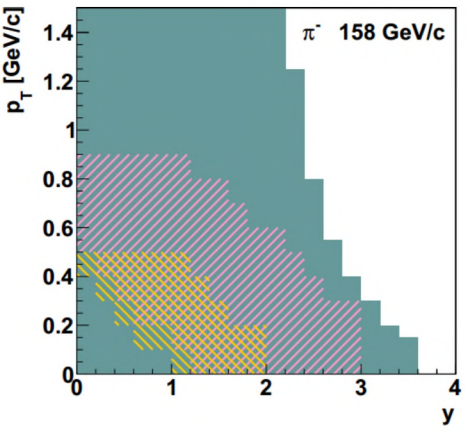

Figure 1. Acceptance for various data analysis methods. Blue, solid area: h^-; magenta lines: dE/dx; yellow lines: time-of-flight.

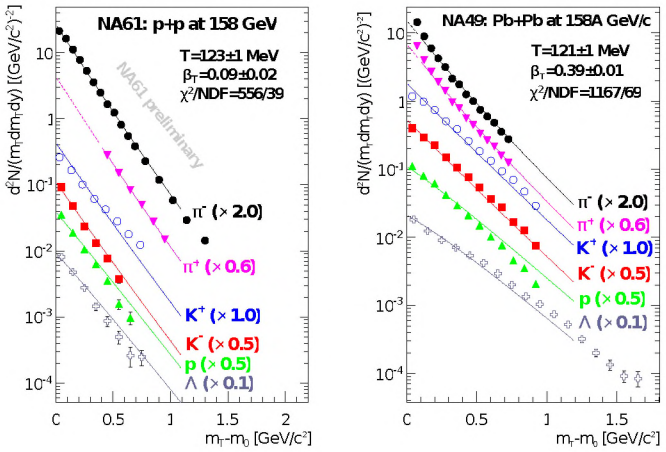

Figure 2. Transverse mass spectra at mid-rapidity. Left: NA61/SHINE inelastic p+p interactions at 158 GeV/c; right: NA49 central Pb+Pb collisions at 158A GeV/c.

3. p+p results

The results presented below were obtained for identified hadrons produced in inelastic p+p interactions at 20, 31, 40, 80 and 158 GeV/c [4].

Figure 2 shows spectra of transverse mass of negatively and positively charged π, K, p and Λ produced in inelastic p+p interactions at mid-rapidity. Corresponding NA49 measurements [5, 6, 7] for central Pb+Pb collisions are also shown. The data was fitted using a blast wave model parametrisation [8] $\frac{dN_i}{m_T dm_T dy} = A_i m_T K_1\left(\frac{m_T \cosh\rho}{T}\right) I_0\left(\frac{p_T \sinh\rho}{T}\right)$. The parameter ρ is related to the transverse flow velocity β_T by $\rho = \tanh^{-1}\beta_T$. One finds that β_T is significantly smaller in p+p than Pb+Pb collisions. While the spectra are approximately exponential in p+p reactions, this exponential dependence is modified in Pb+Pb interactions by the transverse flow.

Figure 3 shows rapidity spectra of π^- produced in inelastic p+p interactions (left), the energy dependence of the rms width σ of those spectra divided by beam rapidity (centre) and divided by predictions (σ_{LS}) from the hydro-dynamical model [9, 10] (right). Although the shapes of the rapidity spectra are approximately Gaussian, the best fit was obtained using a sum of two Gaussians. It can be seen in Figure 3 (centre) that σ/y_{beam} for π^- decreases with increasing collision energy. While σ/σ_{LS} and σ/y_{beam} are smaller in p+p than Pb+Pb collisions, no qualitative difference is observed for their energy dependence.

The "kink", "horn", and "step" [6, 14] are important signals for the onset of deconfinement observed in central Pb+Pb interactions. Figure 4 shows that the energy dependence of mean π multiplicity increases slower in p+p than in Pb+Pb collisions ("kink"). Hence, the two dependences cross each other at around 40A GeV/c.

The new measurements of NA61/SHINE significantly improve the world data for the inverse-slope parameter T of m_T spectra of Kaons [16] and for yields of π^+ mesons at mid-rapidity [17, 18]. The m_T spectra were fitted to the exponential function $\frac{d^2n}{dp_T dy} = \frac{Sp_T}{T^2+m_K T}\exp\left(-\frac{\sqrt{p_T^2+m_K^2}-m_K}{T}\right)$. S is the yield integral and m_K is the K mass. Figure 5 shows the result of the fit to the spectra of K^+ and K^- at mid-rapidity.

Figure 6 shows the energy dependence of T for K^+ and K^-. Surprisingly, the results from inelastic p+p interactions exhibit rapid changes similar to those observed in central Pb+Pb

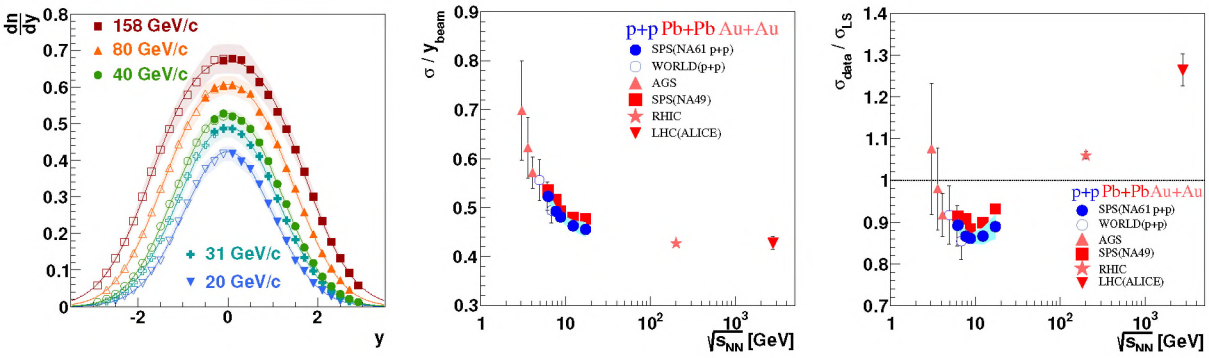

Figure 3. Left: π^- rapidity spectra in inelastic p+p interactions. Centre: energy dependence of the scaled width of rapidity spectra. Right: energy dependence of the ratio of the measured width to that predicted by the hydro-dynamical model [9, 10]. World data from Refs. [11, 12, 13]. Not corrected for isospin effects.

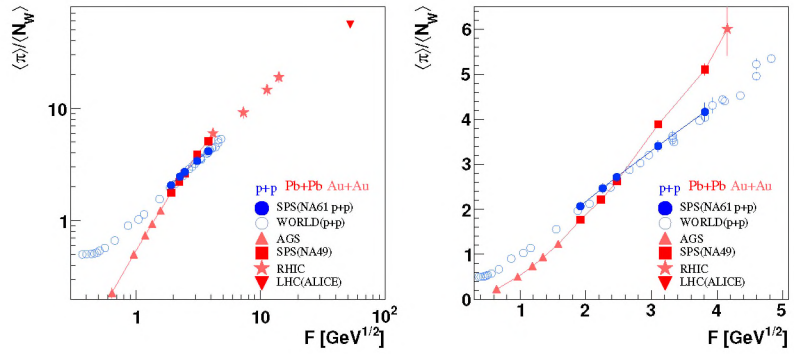

Figure 4. Energy dependence of mean π multiplicity per wounded nucleon in inelastic p+p interactions and central Pb+Pb (Au+Au) collisions. World data from Refs. [12, 15].

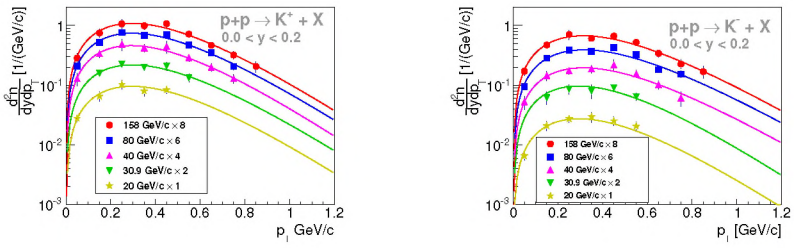

Figure 5. Transverse momentum spectra of K mesons at mid-rapidity in inelastic p+p interactions at CERN SPS energies.

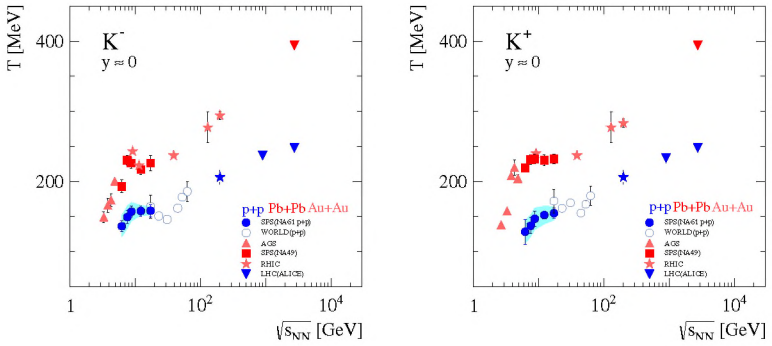

Figure 6. Energy dependence of the inverse slope parameter T of transverse mass spectra of K^+ and K^- in inelastic p+p and central Pb+Pb/Au+Au interactions. World data from Refs. [16, 19, 20, 21].

collisions ("step").

While the h^- method [3] can be used to measure spectra for π^-, a similar approach cannot be used for π^+ because of the large K and p contamination. Instead, the ratio of the measured π^+

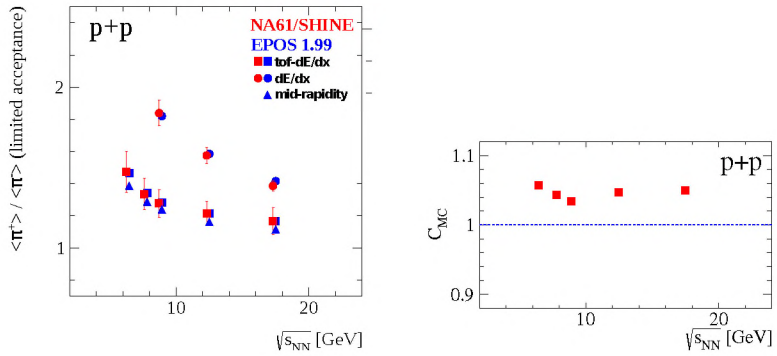

Figure 7. Left: energy dependency of π^+/π^- ratio in inelastic p+p interactions compared with EPOS predictions. Right: correction factors used to obtain π^+ yields from π^- yields.

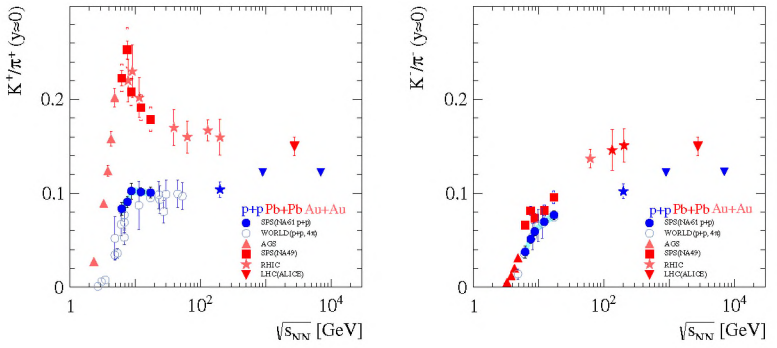

Figure 8. Energy dependence of the K^+/π^+ and K^-/π^- ratios in inelastic p+p and central Pb+Pb and Au+Au interactions. World data from Refs. [15, 17, 18, 21, 22].

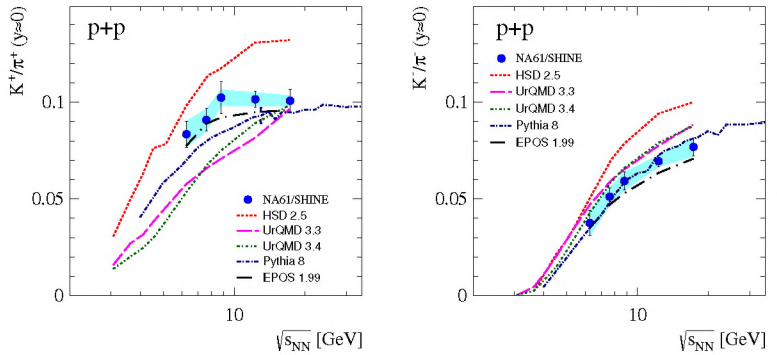

Figure 9. Energy dependence of the K^+/π^+ and K^-/π^- ratios in inelastic p+p interactions compared [23] with theoretical models EPOS [2], UrQMD [24, 25], Pythia 8 [26] and HSD [27].

and π^- yields was calculated within the acceptance of the time-of-flight and/or dE/dx methods, and compared with model predictions. As can be seen in Figure 7 (left), the agreement between the measurements and the EPOS model [2] is better than 0.1%. Finally, the π^+ mid-rapidity yield was calculated as the product of the measured π^- yield at $y = 0$, the measured π^+/π^- ratio within the time-of-flight and dE/dx acceptance, and the EPOS correction factor C_{MC}. This is shown in Figure 7 (right): $\pi^+(y = 0) = \pi^-(y = 0)\pi^+/\pi^-(tof - dE/dx)C_{MC}$, where $C_{MC} = \left[\frac{\pi^+/\pi^-(y=0)}{\pi^+/\pi^-(tof)}\right]_{MC} \approx 5\%$.

Figure 8 shows the energy dependence of the K^+/π^+ and K^-/π^- ratios observed in inelastic p+p interactions, as well as world data for central Pb+Pb and Au+Au interactions as reference. Again surprisingly, the data suggests that even inelastic p+p interactions exhibit a step structure in the energy dependence of the K^+/π^+ ratio, which may be considered a precursor of the "horn" found in central Pb+Pb collisions.

Furthermore, the measured ratios were compared to theoretical models, as shown in Figure 9. It is evident that none of the models adequately describes the data.

Figure 10 shows for protons from inelastic p+p interactions the spectra of p_T (left) and $\langle m_T \rangle$

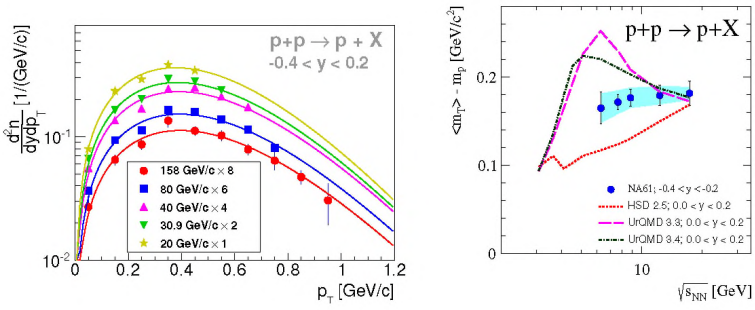

Figure 10. Left: transverse momentum spectra of protons at mid-rapidity in inelastic p+p interactions. Right: comparison of $\langle m_T \rangle - m_p$ calculated using the spectra from the left plot with predictions of models [23].

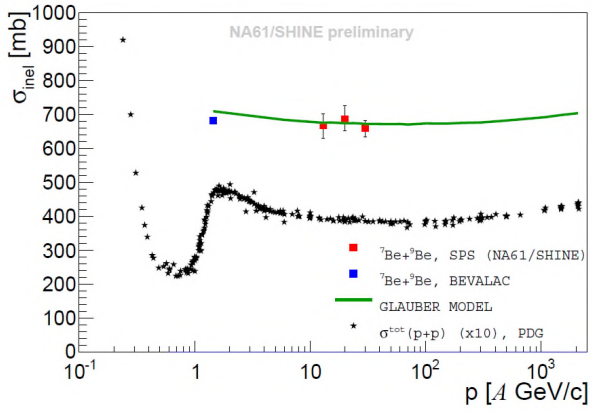

Figure 11. Inelastic cross section of ^{7}Be+^{9}Be collisions as well as total cross section for p+p interactions as a function of beam momentum. The curve shows the prediction of the Glauber model.

(right) as a function of collision energy. Neither the magnitude nor the energy dependence of $\langle m_T \rangle$ is reproduced by the UrQMD or the HSD model.

4. Be+Be results

Previously, the inelastic cross section for ^{7}Be+^{9}Be was only measured at 1.45A GeV/c [28]. The new measurements of NA61/SHINE now extend this to 13A, 20A and 30A GeV/c [29]. A scintillator counter placed behind the target measures the square of the charge of a particle passing through it. Inelastic interactions were selected by requiring a signal below that expected for an intact beam nucleus. Data was also taken with the target removed to be able to subtract the background caused by beam interactions with detector material. The interaction probability is given by $P_{int} = \frac{P_I - P_R}{1 - P_R}$, where P_I and P_R are the interaction probabilities when the target is inserted and removed, respectively. Using P_{int}, the cross section can be calculated from $\sigma_{inel} = \frac{1}{\rho L_{eff} N_A / A} P_{int}$, $L_{eff} = \lambda_{abs}(1 - e^{-L/\lambda_{abs}})$ and $\lambda_{abs} = \frac{A}{\rho N_A \sigma_{inel}}$. N_A, ρ, L and A are the Avogadro constant, the target density, length and atomic number, respectively. Figure 11 shows that the new measurements are in agreement with the previous measurement as well as the Glauber model [30] prediction.

Preliminary results on spectra were obtained for ^{7}Be+^{9}Be interactions at beam momenta of 20A, 30A, 40A, 75A and 150A GeV/c in the centrality classes 0–5%, 5–10%, 10–15% and 15–20% [31]. Unless otherwise stated, only statistical errors are shown. The centrality was derived from the energy deposited in the forward calorimeter PSD. Figure 12 shows the relationship between deposited energy and the centrality classes. Due to the modularity of this detector, it is possible to change the acceptance during off-line analysis. A smaller acceptance will cause some of the projectile spectators to be lost, but at the same time reduces the contribution from particles produced in the collision. Thus, the result will depend on the selected acceptance. This effect is largest for low beam momenta. For example for the total π^- multiplicity at 20A GeV/c, the spread for different acceptances is up to 5%.

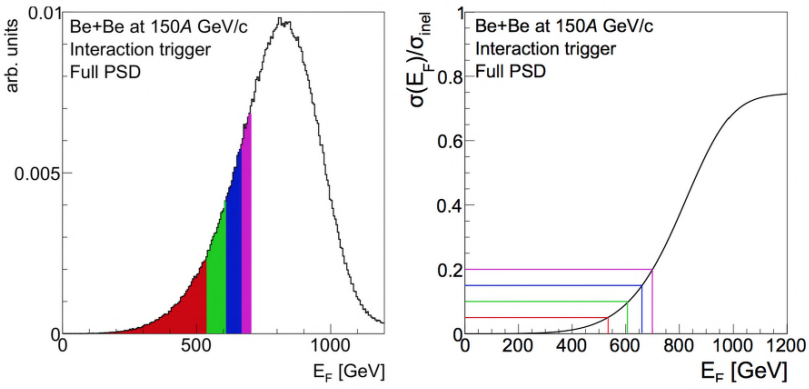

Figure 12. Left: distribution of forward energy E_F measured in the PSD calorimeter in ^{7}Be+^{9}Be collisions at 150A GeV/c. Right: definition of forward energy event classes.

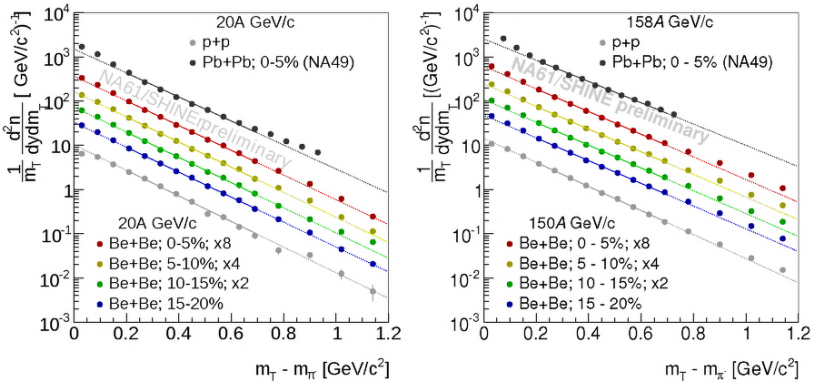

Figure 13. Transverse mass spectra of π^- mesons for ^{7}Be+^{9}Be, p+p and Pb+Pb interactions. Left: 20A GeV/c; right: 150A GeV/c beam momentum.

Figure 13 shows for ^{7}Be+^{9}Be π^- collisions the m_T spectra for the different centrality classes for the beam momenta 20A and 150A GeV/c, as well as for inelastic p+p and central Pb+Pb interactions. The p+p data is described very well by an exponential function, while both ^{7}Be+^{9}Be and Pb+Pb spectra deviate from this function at low and high values of m_T.

Calculating normalised π^- m_T spectra as the ratios (^{7}Be+^{9}Be)/(p+p) and (Pb+Pb)/(p+p) facilitates the comparison of the shapes of the spectra produced in these different size systems. Figure 15 shows qualitatively similar behaviour for both ^{7}Be+^{9}Be and Pb+Pb reactions. The high-m_T regions of both ^{7}Be+^{9}Be and Pb+Pb exhibit an increase of the ratio, while for the intermediate regions a decrease is seen. This effect is stronger for central Pb+Pb collisions. Usually, this is attributed to collective flow. Also, for ^{7}Be+^{9}Be reactions the increase of the ratio at high values of m_T appears to be larger at higher beam momenta. This may suggest an increase of the magnitude of collective effects in ^{7}Be+^{9}Be collisions with increasing beam momentum. The low-m_T regions of both ^{7}Be+^{9}Be and Pb+Pb reactions exhibit an increase of the ratio. Possible explanations include isospin asymmetry of p+p data or electromagnetic effects.

Figure 15 shows the π^- rapidity spectra from ^{7}Be+^{9}Be collisions in the different centrality classes for beam momenta 20A and 150A GeV/c, as well as for inelastic p+p reactions. The data were fitted to two Gaussians symmetrically displaced with respect to mid-rapidity. Although their widths are the same, the amplitudes are different due to the asymmetry of ^{7}Be+^{9}Be collisions. By extending the fit range into the backward rapidity region, it was possible to obtain a stable fit.

The rms width σ_y of the spectra can be obtained from the fitted function. Figure 16 (left) shows the σ_y/y_{beam} for ^{7}Be+^{9}Be, as well as inelastic p+p and central Pb+Pb interactions. The widths of the spectra for all systems decrease monotonically with respect to collision energy. However, the widths of the spectra do not behave monotonically with respect to the system

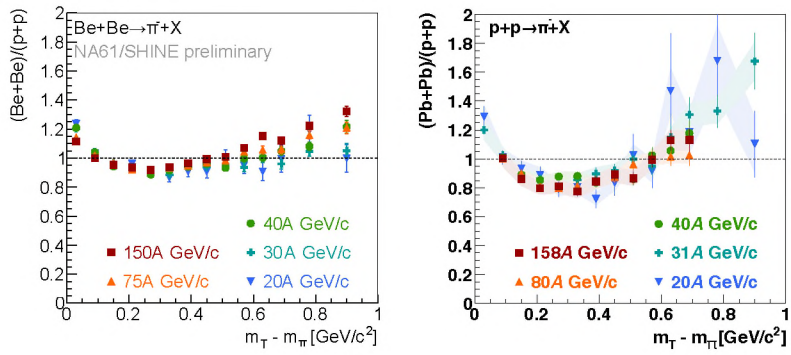

Figure 14. Ratio of normalised transverse mass spectra of π^- mesons for different system sizes. Left: (^{7}Be+^{9}Be)/(p+p); right: (Pb+Pb)/(p+p).

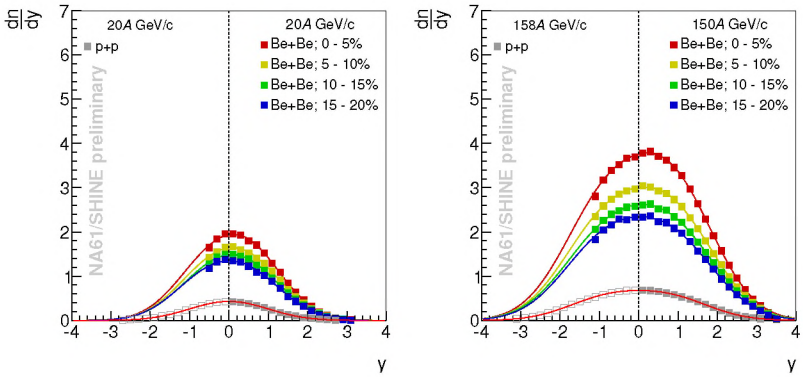

Figure 15. Rapidity spectra of π^- mesons for ^{7}Be+^{9}Be and inelastic p+p interactions. Left: 20A GeV/c; right: 150A GeV/c.

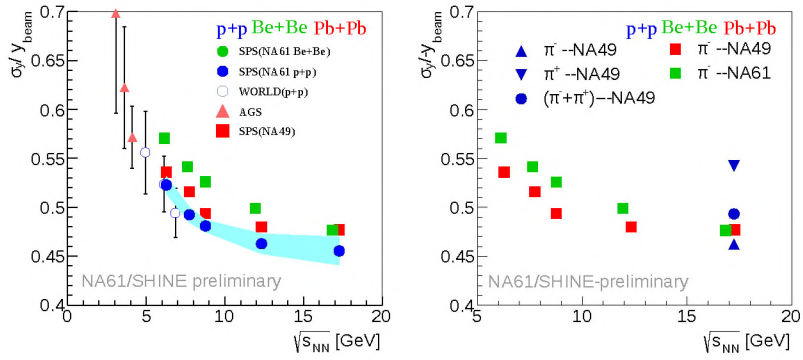

Figure 16. Left: energy dependence of scaled width of ^{7}Be+^{9}Be π^- rapidity spectra; right: effect of isospin asymmetry in p+p interactions. World data from Refs. [7].

size for a given collision energy. The width of the spectra from Pb+Pb lies between those of p+p and ^{7}Be+^{9}Be collisions. When comparing the rapidity spectra from different systems, one must consider that p+p has larger isospin asymmetry than ^{7}Be+^{9}Be and Pb+Pb. This isospin asymmetry can be accounted for by calculating the average spectra for π^- and π^+. The only large-acceptance data available for π^+ production in p+p in the relevant energy domain is from NA49 at 158 GeV/c [32]. Unfortunately, this is also the energy with the smallest differences for the rapidity widths of the different system sizes. Still, Figure 16 (right) shows for 158 GeV/c beam momentum that by taking into account the different isospin asymmetries, the dependence of the rapidity width with respect to system size becomes monotonic.

5. Conclusion

The analysis of inelastic p+p and ^{7}Be+^{9}Be interactions at CERN SPS energies showed many interesting effects. In particular, the p+p data exhibited step-like structures in the energy region where the onset of deconfinement was found in central Pb+Pb collisions. Also, many of the measurements could not be explained well by theoretical models. For ^{7}Be+^{9}Be reactions

new results on the inelastic cross section were obtained at several energies. Transverse mass and rapidity spectra were measured in the SPS energy range for three centrality classes. An indication of a transverse flow effect was found at the highest beam momenta.

Acknowledgements
Supported by the National Science Centre of Poland (grants UMO-2014/13/N/ST2/02565, UMO-2014/12/T/ST2/00692, UMO-2013/11/N/ST2/03879 and UMO-2012/04/M/ST2/00816).

References
[1] N. Abgrall *et al.*, [NA61/SHINE Collab.] *JINST* **9** (2014) P06005, arXiv:1401.4699 [physics.ins-det].
[2] T. Pierog and K. Werner *Nucl.Phys.Proc.Suppl.* **196** (2009) 102–105, arXiv:0905.1198 [hep-ph].
[3] N. Abgrall *et al.*, [NA61/SHINE Collab.] *Eur.Phys.J.* **C74** (2014) 2794, arXiv:1310.2417 [hep-ex].
[4] S. Pulawski, [NA61 Collab.] arXiv:1502.07916 [nucl-ex].
[5] C. Alt *et al.*, [NA49 Collab.] *Phys.Rev.* **C73** (2006) 044910.
[6] C. Alt *et al.*, [NA49 Collab.] *Phys. Rev.* **C77** (2008) 024903.
[7] S. Afanasiev *et al.*, [NA49 Collab.] *Phys. Rev.* **C66** (2002) 054902.
[8] E. Schnedermann, J. Sollfrank, and U. W. Heinz *Phys.Rev.* **C48** (1993) 2462–2475, arXiv:nucl-th/9307020 [nucl-th].
[9] L. Landau *Izv.Akad.Nauk Ser.Fiz.* **17** (1953) 51–64.
[10] E. V. Shuryak *IYF-75-4* (1974) .
[11] J. Klay *et al.*, [E895 Collab.] *Phys. Rev.* **C68** (2003) 054905.
[12] E. Abbas *et al.*, [ALICE Collab.] *Phys.Lett.* **B726** (2013) 610–622, arXiv:1304.0347 [nucl-ex].
[13] S. Adler *et al.*, [PHENIX Collab.] *Phys.Rev.* **C69** (2004) 034909.
[14] M. Gazdzicki, M. Gorenstein, and P. Seyboth *Acta Phys.Polon.* **B42** (2011) 307–351, arXiv:1006.1765 [hep-ph].
[15] B. Abelev *et al.*, [ALICE Collab.] *Phys.Rev.Lett.* **109** (2012) 252301, arXiv:1208.1974 [hep-ex].
[16] M. Kliemant, B. Lungwitz, and M. Gazdzicki *Phys.Rev.* **C69** (2004) 044903, arXiv:hep-ex/0308002 [hep-ex].
[17] M. Gazdzicki and D. Roehrich *Z.Phys.* **C65** (1995) 215.
[18] M. Gazdzicki and D. Rohrich *Z.Phys.* **C71** (1996) 55–64, arXiv:hep-ex/9607004 [hep-ex].
[19] B. Abelev *et al.*, [STAR Collab.] *Phys.Rev.* **C79** (2009) 034909, arXiv:0808.2041 [nucl-ex].
[20] B. B. Abelev *et al.*, [ALICE Collab.] *Phys.Lett.* **B736** (2014) 196–207, arXiv:1401.1250 [nucl-ex].
[21] K. Aamodt *et al.*, [ALICE Collab.] *Eur.Phys.J.* **C71** (2011) 1655, arXiv:1101.4110 [hep-ex].
[22] I. Arsene *et al.*, [BRAHMS Collab.] *Phys.Rev.* **C72** (2005) 014908, arXiv:nucl-ex/0503010 [nucl-ex].
[23] V. Y. Vovchenko, D. Anchishkin, and M. Gorenstein *Phys.Rev.* **C90** no. 2, (2014) 024916, arXiv:1407.0629 [nucl-th].
[24] M. Bleicher *et al. J.Phys.* **G25** (1999) 1859–1896, arXiv:hep-ph/9909407 [hep-ph].
[25] S. Bass *et al. Prog.Part.Nucl.Phys.* **41** (1998) 255–369, arXiv:nucl-th/9803035 [nucl-th].
[26] T. Sjostrand, S. Ask, J. R. Christiansen, R. Corke, N. Desai, *et al. Comput.Phys.Commun.* **191** (2015) 159–177, arXiv:1410.3012 [hep-ph].
[27] W. Ehehalt and W. Cassing *Nucl.Phys.* **A602** (1996) 449–486.
[28] I. Tanihata *et al. Phys. Rev. Lett.* **55** (1985) 2676.
[29] I. Weimer https://edms.cern.ch/file/1308546/1. Bachelor Thesis, Ludwig-Maximilian University Munich.
[30] W. Broniowski, M. Rybczynski, and P. Bozek *Comput.Phys.Commun.* **180** (2009) 69.
[31] E. Kaptur, [NA61/SHINE Collab.] *PoS* **CPOD** (2014) , http://pos.sissa.it/archive/conferences/217/053/CPOD2014_053.pdf.
[32] C. Alt *et al.*, [NA49 Collab.] *Eur. Phys. J.* **C45** (2006) 343.